

# DIPOLE MODEL FOR DOUBLE MESON PRODUCTION IN TWO-PHOTON INTERACTIONS AT HIGH ENERGIES

V.P. Gonçalves <sup>1</sup>, M.V.T. Machado <sup>2,3</sup>

<sup>1</sup> Instituto de Física e Matemática, Universidade Federal de Pelotas  
Caixa Postal 354, CEP 96010-090, Pelotas, RS, Brazil

<sup>2</sup> Universidade Estadual do Rio Grande do Sul - UERGS  
Unidade de Bento Gonçalves. CEP 95700-000. Bento Gonçalves, RS, Brazil

<sup>3</sup> High Energy Physics Phenomenology Group, GFPAE IF-UFRGS  
Caixa Postal 15051, CEP 91501-970, Porto Alegre, RS, Brazil

## ABSTRACT

In this work the double vector meson production in two-photon interactions at high energies is investigated considering saturation physics. We extend the color dipole picture for this process and study the energy and virtuality dependence of the forward differential cross section. Comparison with previous results is presented and the contribution of the different photon polarizations is estimated.

## 1 Introduction

The high energy limit of the perturbative QCD comes from when the center-of-mass is much larger the hard scales present in the problem. In this regime the parton densities inside the projectiles grow with increasing the energy, leading to the growth of the cross sections. As long the energy is not too high, we have low values of the partonic density and the QCD dynamics is described by linear (BFKL/DGLAP) evolution equations [1, 2]. However, at higher energies the parton density increases and the scattering amplitude approach the unitarity limit, where a linear description breaks down and one enters in the saturation regime, where the dynamics is described by a nonlinear evolution equation and the parton densities saturate [3, 4]. The transition line between the linear and nonlinear regimes is characterized by the saturation scale  $Q_{\text{sat}}(x)$ , which is energy dependent and sets the critical transverse size for the unitarization of the cross sections. In other words, unitarity is restored by including nonlinear corrections in the evolution equations. Such effects are small for  $k_{\perp}^2 > Q_{\text{sat}}^2$  and very strong for  $k_{\perp}^2 < Q_{\text{sat}}^2$ , leading to the saturation of the scattering amplitude, where  $k_{\perp}$  is the typical hard scale present in the process. The successful description of all inclusive and diffractive deep inelastic data at the collider HERA by saturation models [5, 6, 7, 8] suggests that these effects might become important in the energy regime probed by current colliders. Furthermore, the saturation model has been extended to two-photon interactions at high energies in Ref. [9], also obtaining a very

good description of the data on the  $\gamma\gamma$  total cross section, on the photon structure function at low  $x$  and on the  $\gamma^*\gamma^*$  cross section. The formalism used in Ref. [9] is based on the dipole picture [10], with the  $\gamma^*\gamma^*$  total cross sections being described by the interaction of two color dipoles, which the virtual photons fluctuate into (For previous analysis using the dipole picture see, e.g., Refs. [11, 12]). The dipole-dipole cross section is modeled considering the saturation physics. The successful descriptions of the experimental data on the  $\gamma\gamma$  interactions and on light and heavy vector meson production for  $ep$  collisions at HERA are our main motivations to extend this formalism to describe the double meson production and analyze the effects of the saturation physics in this process.

In the last few years the double meson production has been studied considering different approaches and approximations for the QCD dynamics [12, 13, 14, 15, 16, 17, 18, 19, 20]. In particular, in our previous paper in Ref. [15], we have performed a phenomenological analysis for the double  $J/\Psi$  production using the forward LLA BFKL solution. In that case, the hard scale was set by the charm quark mass. There, we also studied the possible effects of corrections at next to leading approximation (NLA) level to the BFKL kernel investigating the slow down of the effective hard Pomeron intercept. Afterwards, in Ref. [17] the non-forward solution was considered for a larger set of possible vector meson pairs, where the large  $t$  values provide the perturbative scale. Moreover, in that paper the double vector meson production in real photon interactions was studied, the  $t$ -dependence of the differential cross section was analyzed in detail and the total cross section for different combinations of vector mesons was calculated using the leading order impact factors and BFKL amplitude. More recently, two other studies on the process  $\gamma^*\gamma^* \rightarrow VV$  has appeared in literature [19, 20]. In the first one [19], the leading order BFKL amplitude for the exclusive diffractive two- $\rho$  production in the forward direction is computed and the NLA corrections are estimated using a specific resummation of higher order effects. In the last paper [20], the amplitude for the forward electroproduction of two light vector mesons in NLA is computed. In particular, the NLA amplitude is constructed by the convolution of the  $\gamma^* \rightarrow V$  impact factor and the BFKL Green's function in the  $\overline{\text{MS}}$  scheme. In addition, a procedure to get results independent from the energy and renormalization scales has been investigated within NLA approximation. A shortcoming of these approaches is that it consider only the linear regime of the QCD dynamics and disregard that nonlinear effects, associated to the saturation physics, can be present. However, double meson production in two photon interactions at high energies offer an ideal opportunity for the study of the transition between the linear and saturation regimes since virtualities of both photons in the initial state can vary as well as the vector mesons in the final state. While for the interaction of two highly virtual photons and/or double heavy vector meson production we expect the dominance of hard physics (linear regime), in the opposite regime, characterized by the double light vector meson production by the interaction of two real photons, the soft physics is expected to be dominant. Consequently, in an intermediate scenario, we may expect that the main contribution comes from semi-hard physics, determined by saturation effects.

In this paper we derive the main formulae to describe the double meson production in the dipole picture and analyze the double meson production in two photon interactions considering three cases of physical and phenomenological interest: (a) the interaction of two real photons, and the interaction of two virtual photons with (b) equal and (c) different virtualities. In all

cases we calculate the forward differential cross section for the  $\rho\rho$ ,  $\rho J/\Psi$  and  $J/\Psi J/\Psi$  production. Moreover, we present a comparison between the linear and nonlinear predictions and estimate the contribution of the distinct photon polarizations.

## 2 Basic Formulae

### 2.1 Double meson production in the dipole picture

Let us introduce the main formulae concerning the vector meson production in the color dipole picture. First, we consider the scattering process  $\gamma\gamma \rightarrow V_1 V_2$ , where  $V_i$  stands for both light and heavy mesons. At high energies, the scattering process can be seen as a succession in time of three factorizable subprocesses: i) the photon fluctuates in quark-antiquark pairs (the dipoles), ii) these color dipoles interact and, iii) the pairs convert into the vector mesons final states. Using as kinematic variables the  $\gamma^*\gamma^*$  c.m.s. energy squared  $s = W^2 = (p + q)^2$ , where  $p$  and  $q$  are the photon momenta, the photon virtualities squared are given by  $Q_1^2 = -q^2$  and  $Q_2^2 = -p^2$  and the Bjorken variable is defined by

$$x_{12} = \frac{Q_1^2 + Q_2^2 + M_{V_1}^2 + M_{V_2}^2}{W^2 + Q_1^2 + Q_2^2}. \quad (1)$$

The corresponding imaginary part of the amplitude at zero momentum transfer reads as

$$\begin{aligned} \text{Im } \mathcal{A}(\gamma^*\gamma^* \rightarrow V_1 V_2) &= \sum_{h, \bar{h}} \sum_{n, \bar{n}} \int dz_1 d^2\mathbf{r}_1 \Psi_{h, \bar{h}}^\gamma(z, \mathbf{r}_1, Q_1^2) \Psi_{h, \bar{h}}^{V_1^*}(z_1, \mathbf{r}_1) \\ &\times \int dz_2 d^2\mathbf{r}_2 \Psi_{n, \bar{n}}^\gamma(z_2, \mathbf{r}_2, Q_2^2) \Psi_{n, \bar{n}}^{V_2^*}(z_2, \mathbf{r}_2) \sigma_{dd}(x_{12}, \mathbf{r}_1, \mathbf{r}_2), \end{aligned} \quad (2)$$

where  $\Psi^\gamma$  and  $\Psi^{V_i}$  are the light-cone wavefunctions of the photon and vector meson, respectively. The quark and antiquark helicities are labeled by  $h, \bar{h}, n$  and  $\bar{n}$  and reference to the meson and photon helicities are implicitly understood. The variable  $\mathbf{r}_1$  defines the relative transverse separation of the pair (dipole) and  $z_1 (1 - z_1)$  is the longitudinal momentum fractions of the quark (antiquark). Similar definitions are valid for  $\mathbf{r}_2$  and  $z_2$ . The basic blocks are the photon wavefunction,  $\Psi^\gamma$ , the meson wavefunction,  $\Psi_{T,L}^V$ , and the dipole-dipole cross section,  $\sigma_{dd}$ .

In the dipole formalism, the light-cone wavefunctions  $\Psi_{h, \bar{h}}(z, \mathbf{r})$  in the mixed representation  $(\mathbf{r}, z)$  are obtained through two dimensional Fourier transform of the momentum space light-cone wavefunctions  $\Psi_{h, \bar{h}}(z, \mathbf{k})$  (see more details, e.g. in Refs. [21, 22, 23]). The normalized light-cone wavefunctions for longitudinally ( $L$ ) and transversely ( $T$ ) polarized photons are given by:

$$\Psi_{h, \bar{h}}^L(z, \mathbf{r}) = \sqrt{\frac{N_c}{4\pi}} \delta_{h, -\bar{h}} e e_f 2z(1-z) Q \frac{K_0(\varepsilon r)}{2\pi}, \quad (3)$$

$$\Psi_{h, \bar{h}}^{T(\gamma=\pm)}(z, \mathbf{r}) = \pm \sqrt{\frac{N_c}{2\pi}} e e_f \left[ i e^{\pm i\theta_r} (z \delta_{h\pm, \bar{h}\mp} - (1-z) \delta_{h\mp, \bar{h}\pm}) \partial_r + m_f \delta_{h\pm, \bar{h}\pm} \right] \frac{K_0(\varepsilon r)}{2\pi}, \quad (4)$$

where  $\varepsilon^2 = z(1-z)Q^2 + m_f^2$ . The quark mass  $m_f$  plays a role of a regulator when the photoproduction regime is reached. Namely, it prevents non-zero argument for the modified Bessel functions  $K_{0,1}(\varepsilon r)$  towards  $Q^2 \rightarrow 0$ . The electric charge of the quark of flavor  $f$  is given by  $e e_f$ .

For vector mesons, the light-cone wavefunctions are not known in a systematic way and they are thus obtained through models. The simplest approach assumes a same vector current as in the photon case, but introducing an additional vertex factor. Moreover, in general a same functional form for the scalar part of the meson light-cone wavefunction is chosen. Here, we follow the analytically simple DGKP approach [24]. In this particular approach, one assumes that the dependencies on  $\mathbf{r}$  and  $z$  of the wavefunction are factorised, with a Gaussian dependence on  $\mathbf{r}$ . Its main shortcoming is that it breaks the rotational invariance between transverse and longitudinally polarized vector mesons [25]. However, as it describes reasonably the HERA data for vector meson production, as pointed out in Refs. [23, 26], we will use it in our phenomenological analysis. The DGKP longitudinal and transverse meson light-cone wavefunctions are given by [24],

$$\Psi_{h,\bar{h}}^{V,L}(z, \mathbf{r}) = z(1-z) \delta_{h,-\bar{h}} \frac{\sqrt{\pi} f_V}{2\sqrt{N_c} \hat{e}_f} f_L(z) \exp\left[\frac{-\omega_L^2 \mathbf{r}^2}{2}\right], \quad (5)$$

$$\begin{aligned} \Psi_{h,\bar{h}}^{V,T(\gamma=\pm)}(z, \mathbf{r}) &= \pm \left( \frac{i\omega_T^2 r e^{\pm i\theta_r}}{m_V} [z\delta_{h\pm,\bar{h}\mp} - (1-z)\delta_{h\mp,\bar{h}\pm}] + \frac{m_f}{m_V} \delta_{h\pm,\bar{h}\pm} \right) \\ &\quad \times \frac{\sqrt{\pi} f_V}{\sqrt{2N_c} \hat{e}_f} f_T(z) \exp\left[\frac{-\omega_T^2 \mathbf{r}^2}{2}\right], \end{aligned} \quad (6)$$

where  $\hat{e}_f$  is the effective charge arising from the sum over quark flavors in the meson of mass  $m_V$ . The following values  $\hat{e}_f = 1/\sqrt{2}$  and  $2/3$  stand for the  $\rho$  and  $J/\Psi$ , respectively. The coupling of the meson to electromagnetic current is labeled by  $f_V^2 = 3 m_V \Gamma_{e^+e^-} / 4 \pi \alpha_{em}^2$  (see Table 1). The function  $f_{T,L}(z)$  is given by the Bauer-Stech-Wirbel model [27]:

$$f_{T,L}(z) = \mathcal{N}_{T,L} \sqrt{z(1-z)} \exp\left[\frac{-m_V^2 (z-1/2)^2}{2\omega_{T,L}^2}\right]. \quad (7)$$

The meson wavefunctions are constrained by the normalization condition, which contains the hypothesis of a meson composed only of quark-antiquark pairs, and by the electronic decay width  $\Gamma_{V \rightarrow e^+e^-}$ . Both conditions are respectively given by [28, 22],

$$\sum_{h,\bar{h}} \int d^2\mathbf{r} dz |\Psi_{h,\bar{h}}^{V(\lambda)}(z, \mathbf{r})|^2 = 1, \quad (8)$$

$$\sum_{h,\bar{h}} \int \frac{d^2\mathbf{r}}{(2\pi)^2} \frac{dz}{z(1-z)} [z(1-z)Q^2 + k^2 + m_f^2] \Psi_{h,\bar{h}}^V(k, z) \Psi_{h,\bar{h}}^{\gamma*}(k, z) = e f_V m_V (\varepsilon_\gamma^* \cdot \varepsilon_V). \quad (9)$$

The above constraints when used on the DGKP wavefunction produce the following relations [23],

$$\omega_{L,T} = \frac{\pi f_V}{\sqrt{2N_c} \hat{e}_f} \sqrt{I_{L,T}}, \quad (10)$$

$V(m_V)$ MeV	$\hat{e}_V$	$f_V$ [GeV]	$\omega_T$ [GeV]	$\mathcal{N}_T$	$\omega_L$ [GeV]	$\mathcal{N}_L$
$\rho(770)$	$1/\sqrt{2}$	0.153	0.218	8.682	0.331	15.091
$J/\Psi(3097)$	$2/3$	0.270	0.546	7.665	0.680	19.350

Table 1: Parameters and normalization of the DGKP vector meson light-cone wavefunctions. Results obtained using quark mass values from the saturation model (see text).

$$\int_0^1 dz z(1-z) f_L(z) = \int_0^1 dz \frac{2[z^2 + (1-z)^2] \omega_T^2 + m_f^2}{2m_V^2 z(1-z)} f_T(z) = 1, \quad (11)$$

where

$$I_L = \int_0^1 dz z^2(1-z)^2 f_L^2(z), \quad (12)$$

$$I_T = \int_0^1 dz \frac{[z^2 + (1-z)^2] \omega_T^2 + m_f^2}{m_V^2} f_T^2(z). \quad (13)$$

The relations in Eq. (10) come from the normalization condition, whereas the relations in Eq. (11) are a consequence of the leptonic decay width constraints. The parameters  $\omega_{T,L}$  and  $\mathcal{N}_{T,L}$  are determined by solving (10) and (11) simultaneously. In Table 1 we quote the results which will be used in our further analysis. To be consistent with the saturation models, which we will discuss further, we have used the quark masses  $m_{u,d,s} = 0.14$  GeV and  $m_c = 1.5$  GeV. We quote Refs. [23, 26] for more details in the present approach and its comparison with data for both photo and electroproduction of vector mesons.

Finally, the imaginary part of the forward amplitude can be obtained by putting the expressions for photon and vector meson (DGKP) wavefunctions, Eqs. (3-4) and (5-6), into Eq. (2). Moreover, summation over the quark/antiquark helicities and an average over the transverse polarization states of the photon should be taken into account. In order to obtain the total cross section, we assume an exponential parameterization for the small  $|t|$  behavior of the amplitude. After integration over  $|t|$ , the total cross section for double vector meson production by real/virtual photons in two photon interactions case reads as,

$$\sigma(\gamma\gamma \rightarrow V_1 V_2) = \frac{1}{B_{V_1 V_2}} \left. \frac{d\sigma(\gamma\gamma \rightarrow V_1 V_2)}{dt} \right|_{t_{min}=0} = \frac{[\mathcal{I}m \mathcal{A}(s, t=0)]^2}{16\pi B_{V_1 V_2}} (1 + \beta^2) \quad (14)$$

where  $\beta$  is the ratio of real to imaginary part of the amplitude and  $B_{V_1 V_2}$  labels the slope parameter.

## 2.2 Dipole-dipole cross section in the saturation model

The dipole formulation has been extensively used in the description of inclusive and diffractive processes at HERA in an unified way, with the basic quantity being the the dipole-proton cross

section  $\sigma_{dip}$ , which contains all information about the target and the strong interaction physics. In general, the saturation models [5, 6, 7, 8] interpolate between the small and large dipole configurations, providing color transparency behavior,  $\sigma_{dip} \sim \mathbf{r}^2$ , as  $\mathbf{r} \ll 1/Q_{\text{sat}}$  and constant behavior at large dipole separations  $\mathbf{r} > 1/Q_{\text{sat}}$ . The physical scale giving the the transition between the a dilute and a saturated system is named saturation scale,  $Q_{\text{sat}} \propto x^{-\lambda}$ , which is energy dependent. Along these lines, the phenomenological saturation model proposed by Golec-Biernat and Wusthoff (GBW) [5] resembles the main features of the Glauber-Mueller resummation. Namely, the dipole cross section in the GBW model takes the eikonal-like form,

$$\sigma_{dip}^{\text{GBW}}(x, \mathbf{r}) = \sigma_0 \left[ 1 - \exp \left( -\frac{Q_{\text{sat}}^2(x) \mathbf{r}^2}{4} \right) \right]. \quad (15)$$

Its phenomenological application has been successful in a wide class of processes with a photon probe. Although the GBW model describes reasonably well the HERA data, its functional form is only an approximation of the theoretical nonlinear QCD approaches [3, 4]. In Ref. [8] a parameterization for the dipole cross section was constructed to smoothly interpolate between the limiting behaviors analytically under control: the solution of the BFKL equation for small dipole sizes,  $\mathbf{r} \ll 1/Q_{\text{sat}}(x)$ , and the Levin-Tuchin law [29] for larger ones,  $\mathbf{r} \gg 1/Q_{\text{sat}}(x)$ . A fit to the structure function  $F_2(x, Q^2)$  was performed in the kinematical range of interest, showing that it is not very sensitive to the details of the interpolation. The dipole cross section was parameterized as follows,

$$\sigma_{dip}^{\text{IIM}}(x, \mathbf{r}) = \sigma_0 \begin{cases} \mathcal{N}_0 \left( \frac{\mathbf{r} Q_{\text{sat}}}{2} \right)^{2 \left( \gamma_{\text{sat}} + \frac{\ln(2/\mathbf{r} Q_{\text{sat}})}{\kappa \lambda Y} \right)}, & \text{for } \mathbf{r} Q_{\text{sat}}(x) \leq 2, \\ 1 - \exp \left[ -a \ln^2 (b \mathbf{r} Q_{\text{sat}}) \right], & \text{for } \mathbf{r} Q_{\text{sat}}(x) > 2, \end{cases} \quad (16)$$

where the expression for  $\mathbf{r} Q_{\text{sat}}(x) > 2$  (saturation region) has the correct functional form, as obtained either by solving the Balitsky-Kovchegov (BK) equation [3], or from the theory of the Color Glass Condensate (CGC) [4]. Hereafter, we label the model above by IIM. The coefficients  $a$  and  $b$  are determined from the continuity conditions of the dipole cross section at  $\mathbf{r} Q_{\text{sat}}(x) = 2$ . The coefficients  $\gamma_{\text{sat}} = 0.63$  and  $\kappa = 9.9$  are fixed from their LO BFKL values. In our further calculations it will be used the parameters  $R_p = 0.641$  fm,  $\lambda = 0.253$ ,  $x_0 = 0.267 \times 10^{-4}$  and  $\mathcal{N}_0 = 0.7$ , which give the best fit result. It is important to emphasize that the GBW and IIM saturation models are suitable in the region below  $x = 0.01$  and the large  $x$  limit needs still a consistent treatment. At  $ep$  collisions the dipole-proton cross sections should be supplemented by a threshold factor  $(1-x)^{n_{\text{thres}}}$ , taking  $n_{\text{thres}} = 5$  for a 3-flavor analysis and  $n_{\text{thres}} = 7$  for a 4-flavor one.

Following Ref. [9] we can extend the saturation model, originally proposed to describe  $ep$  collisions, to two-photon interactions at high energies. The basic idea is that the dipole-dipole cross section  $\sigma_{dd}(x, \mathbf{r}, \mathbf{r}')$  has the same functional form as the dipole-proton one and is expressed in terms of an effective radius  $\mathbf{r}_{\text{eff}}$ , which depends on  $\mathbf{r}_1$  and/or  $\mathbf{r}_2$ . Consequently, we have that [9],

$$\sigma_{dd}^{\text{GBW}}(x_{12}, \mathbf{r}_{\text{eff}}) = \hat{\sigma}_0 \left[ 1 - \exp \left( -\frac{Q_{\text{sat}}^2(x_{12}) \mathbf{r}_{\text{eff}}^2}{4} \right) \right], \quad (17)$$

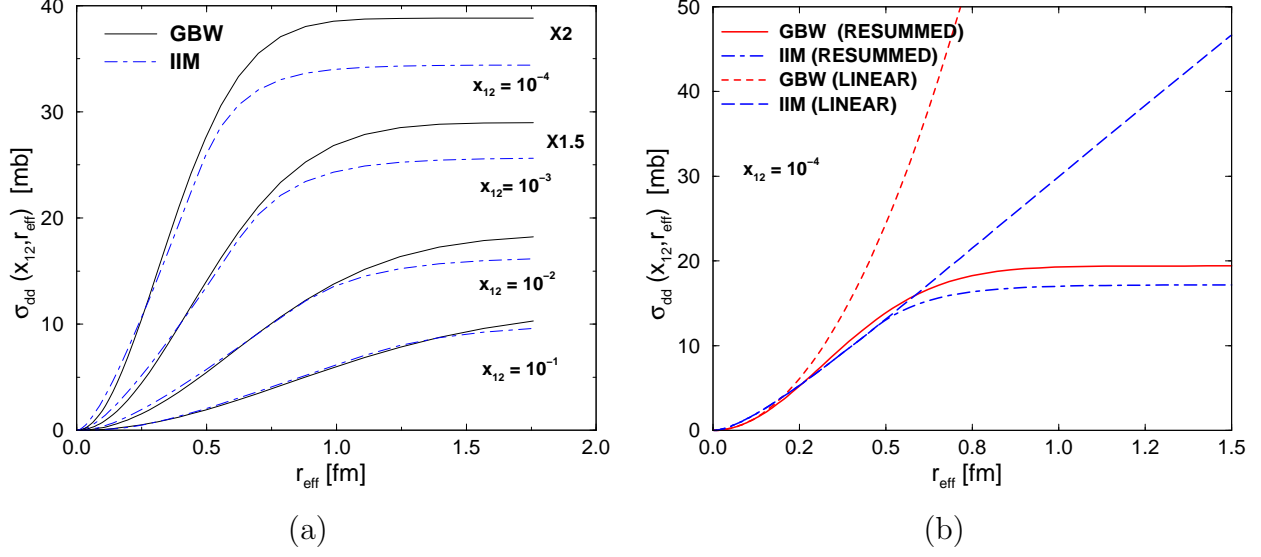


Figure 1: Dipole-dipole cross sections: (a) Comparison between the predictions for GBW and IIM models at different values of  $x_{12}$ . (b) Comparison between their resummed predictions and the corresponding linear limits.

and

$$\sigma_{dd}^{\text{IIM}}(x_{12}, \mathbf{r}_{\text{eff}}) = \hat{\sigma}_0 \begin{cases} \mathcal{N}_0 \left( \frac{\mathbf{r}_{\text{eff}} Q_{\text{sat}}}{2} \right)^2 \left( \gamma_{\text{sat}} + \frac{\ln(2/\mathbf{r}_{\text{eff}} Q_{\text{sat}})}{\kappa \lambda Y} \right), & \text{for } \mathbf{r}_{\text{eff}} Q_{\text{sat}}(x_{12}) \leq 2, \\ 1 - \exp \left[ -a \ln^2 (b \mathbf{r}_{\text{eff}} Q_{\text{sat}}) \right], & \text{for } \mathbf{r}_{\text{eff}} Q_{\text{sat}}(x_{12}) > 2, \end{cases} \quad (18)$$

where the Bjorken  $x_{12}$  variable is given by the Eq. (1) and  $\hat{\sigma}_0 = \frac{2}{3}\sigma_0$ , with  $\sigma_0$  the same as in Refs. [5] and [8]. The last relation can be justified in terms of the quark counting rule. In Ref. [9] three different scenarios for  $\mathbf{r}_{\text{eff}}$  has been considered, with the dipole-dipole cross section presenting in all cases the color transparency property ( $\sigma_{dd} \rightarrow 0$  for  $\mathbf{r}_1 \rightarrow 0$  or  $\mathbf{r}_2 \rightarrow 0$ ) and saturation ( $\sigma_{dd} \rightarrow \hat{\sigma}_0$ ) for large size dipoles. In what follows, we use the model I from [9], where  $\mathbf{r}_{\text{eff}}^2 = \mathbf{r}_1^2 \mathbf{r}_2^2 / (\mathbf{r}_1^2 + \mathbf{r}_2^2)$ , which is favoured by the  $\gamma^* \gamma^*$  and  $F_2^\gamma$  data. We have tested the sensitivity of the result to a different prescription,  $\mathbf{r}_{\text{eff}}^2 = \min(\mathbf{r}_1^2, \mathbf{r}_2^2)$  (named model II in Ref. [9]). Its deviation from model I is quite large for  $\rho$  production and almost insensitive for the mixed  $\rho J/\Psi$  production. For double  $J/\Psi$  production the deviation is considerably larger than the mixed one. However, the difference concerns only to the overall normalization and no change is seen in the energy behavior. Moreover, in order to extend the dipole model to large  $x_{12}$  it is necessary to taken into account threshold correction factors which constrain that the cross section vanish when  $x_{12} \rightarrow 1$  as a power of  $1 - x_{12}$ . As in Ref. [9], we multiply the dipole-dipole cross section by the factor  $(1 - x_{12})^5$ .

A comment is in order here. One shortcoming of the GBW model is that it does not contain the correct DGLAP limit at large virtualities. Consequently, we may expect that its predictions are only valid at small values of the photon virtualities. Therefore, in what follows we only consider photon virtualities up to  $10 \text{ GeV}^2$ . Another aspect which should be emphasized is that the saturation models proposed in Refs. [6, 7, 8] obtain a better description of the  $ep$  HERA

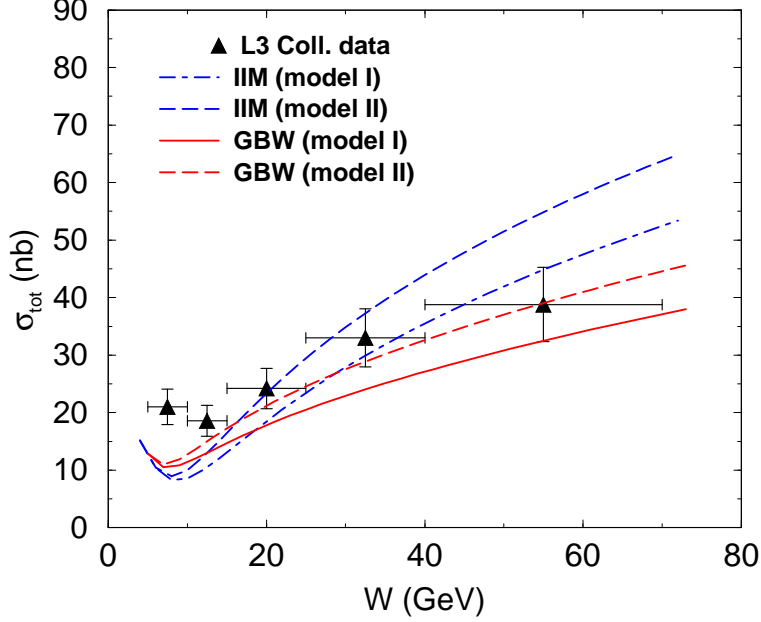


Figure 2: A comparison between the results for GBW and IIM dipole-dipole cross section for charm production in two real photon collisions. The QPM contribution has been added. Data from L3 Collaboration.

data. However, as the unique model which was extended for  $\gamma\gamma$  interactions and its predictions compared with experimental data was the GBW model, we will consider this model in what follows. We postpone for a future publication a detailed analyzes of this reaction considering the DGLAP evolution in the saturation model.

In Fig. 1 (a) we present the dependence of the two dipole-dipole cross sections, Eqs. (17) and (18), as a function the effective radius  $r_{\text{eff}}$  at different values of  $x_{12}$  ( $x_{12} = 10^{-n}$ ,  $n = 1, 2, 3, 4$ ). We have that at small values of  $r_{\text{eff}}$  their behavior are similar, while it differs approximately 15 % at large  $r_{\text{eff}}$  and small values of  $x_{12}$ . In order to emphasize the importance of the saturation effects, in Fig. 1-b we present a comparison between the full predictions of the GBW and IIM dipole-dipole cross sections and its linear limits. We have named as resummed the curves with the complete expressions in Eqs. (17-18) and linear the approximations of them in the limit of small dipoles. Namely, for the linear case one has  $\sigma_{dd}^{\text{GBW}} \propto \hat{\sigma}_0(Q_{\text{sat}}^2 r_{\text{eff}}^2/4)$  and for the IIM model we just take the extrapolation of Eq. (18) for  $r_{\text{eff}} \leq 2/Q_{\text{sat}}$ . We have that at  $r_{\text{eff}} \approx 0.2$  fm the linear and resummed predictions from the GBW model starts to be different. On the other hand, in the IIM case, this difference starts at  $r_{\text{eff}} \approx 0.5$  fm. Consequently, the transition between the linear and saturation regimes is distinct in the GBW and IIM models. This features will have direct implications in the behavior on energy and virtuality of the total cross sections.

In next section we will compare the predictions for the double meson production coming from different models for the dipole-dipole cross section. However, the extension of the IIM model for the photon-photon interactions has not been considered before. For sake of completeness,



we compare the GBW and IIM models for the specific case of heavy quark production. This is motivated by its relation with the double  $J/\Psi$  production. The GBW model has already been considered in Ref. [9], while the IIM result is the first one in literature. We compute the cross section for charm production in the reaction  $\gamma\gamma \rightarrow c\bar{c}$ , considering real photons. The results are presented in Fig. 2 for two prescriptions of the effective radius (model I and II referred before) and compared with L3 data. The the low energy quark box contribution (QPM) has been added. An additional contribution, which we do not include, is the resolved (single and double) piece to the charm cross section, which reaches 30 % of the main contribution at high energies. As already verified in Ref. [9], both prescriptions for the effective radius give reasonable data description when the GBW saturation model is considered. On the other hand, in the IIM model, the model I for the effective radius gives a better description, with the model II overestimating the L3 data at high energies. Moreover, the IIM model implies a stronger energy dependence of the heavy quark production cross section than the GBW prediction. This behavior should also be present in other processes characterized by a hard scale as, for instance, the interaction of two highly virtual photons or double heavy vector meson production. In what follows we only will consider the model I for the effective radius.

### 3 Results

In order to calculate the total cross section for double vector meson production given in Eq. (14) it is necessary to specify the value of the slope parameter  $B_{V_1 V_2}$ . As this quantity is not well constrained, in what follows we only will present our predictions for the energy and virtuality dependence of the forward differential cross section  $\left. \frac{d\sigma(\gamma\gamma \rightarrow V_1 V_2)}{dt} \right|_{t_{min}=0}$ . This should be enough for the present level of accuracy. We start by the scattering of two real photons, investigating its dependence on energy and on the mesons mass. After, we consider the scattering of virtual photons and investigate the symmetric ( $Q_1^2 = Q_2^2$ ) and asymmetric ( $Q_1^2 \propto \alpha Q_2^2$  with  $\alpha \gg 1$ ) cases. In addition, we estimate the magnitude of the contribution of the distinct polarizations for the total cross sections. Finally, we discuss the effect of parton saturation effects in the production of the different mesons.

#### 3.1 Double meson production on real photons interactions

Lets start our analyzes considering the double meson production in two real photon scattering. In Fig. 3 we present the forward differential cross sections for the representative cases of double  $\rho$ ,  $\rho J/\Psi$  and double  $J/\Psi$  in the energy range  $50 \text{ GeV} \leq W_{\gamma\gamma} \leq 10^3 \text{ GeV}$ . The curves are presented for the two models of the dipole-dipole cross section given in Eqs. (17) and (18). Bold curves stand for GBW model and thin curves for IIM model. The forward differential cross section is sizeable in the double  $\rho$  case, being of order 20-40 nb/GeV<sup>2</sup> in the energy range considered. The mixed  $\rho J/\Psi$  production comes as the second higher rate reaching 4 – 40 pb/GeV<sup>2</sup>, whereas double  $J/\Psi$  production is quite low. The deviations between the GBW and IIM models are large for the double  $\rho$  production, with IIM results being a factor 10 below

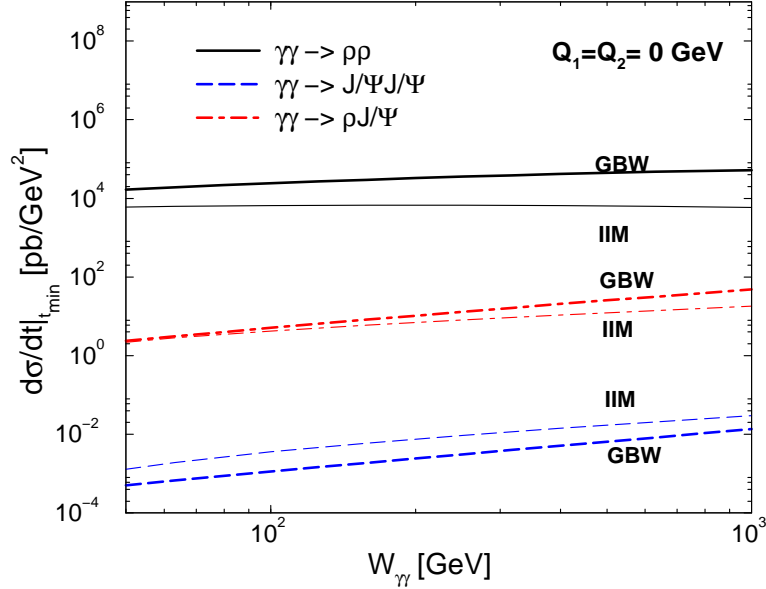


Figure 3: Energy dependence of the forward differential cross section for double vector meson production considering real photons interactions ( $Q_1^2 = Q_2^2 = 0 \text{ GeV}^2$ ). Bold (thin) curves are the results for GBW (IIM) parameterization for dipole-dipole cross section.

GBW towards 1 TeV, which is directly associated to smaller dipole-dipole cross section of the IIM model in the saturation regime [See Fig. 1 (b)]. For the double  $J/\Psi$  production, the IIM prediction overestimates the GBW one by a factor 4, which agrees with the expectation which comes from our previous results for heavy quark production (See Fig. 2). On the other hand, in the  $\rho J/\Psi$  case, the results are equivalent at low energies but differ a factor two at 1 TeV, with the GBW prediction being greater than the IIM one. These features can be qualitatively understood based on the scales involved in the process. As we discussed before, IIM dipole-dipole cross section has a relatively faster transition to saturation in comparison with GBW model and underestimates it by a factor of 20-30% at small- $x_{12}$ . In double  $\rho$  and mixed vector meson production the typical scale is given by the light meson mass  $\bar{\mu}^2 = 2M_\rho^2$  or the sum of light-heavy meson  $\bar{\mu}^2 = (M_\rho^2 + M_{J/\Psi}^2)$ . Therefore, those processes are dominated by a relatively soft scale and saturation effects should be important. On the other hand, in the double  $J/\Psi$  production the typical scale is sufficiently hard,  $\bar{\mu}^2 = 2M_{J/\Psi}^2$ . Therefore, we expect a larger contribution of small dipoles leading to a cross section with higher magnitude.

In order to analyze the energy dependence for each forward differential cross section we have performed a simple power-like fit in the energy interval  $50 \leq W_{\gamma\gamma} \leq 10^3 \text{ GeV}$  in the form  $\left. \frac{d\sigma_{V_1 V_2}}{dt} \right|_{t_{min}=0} \propto W_{\gamma\gamma}^\alpha$ . For the double  $\rho$  production one obtains  $\alpha = 0.4$  (0.08) for GBW (IIM) model. In Regge phenomenology, this corresponds to an effective Pomeron intercept of order  $\alpha_P^{\text{eff}} \approx \alpha/4 = 0.1$  (0.02) for GBW (IIM) parameterizations, which is clearly a soft behavior. This fact shows that the IIM model contains stronger saturation effects in contrast to GBW one in the case of dominantly soft scales. In the mixed production, the effective power increases to  $\alpha = 0.96$  (0.65) for GBW (IIM) models and the deviation is not too sizeable as in the  $\rho$  case.

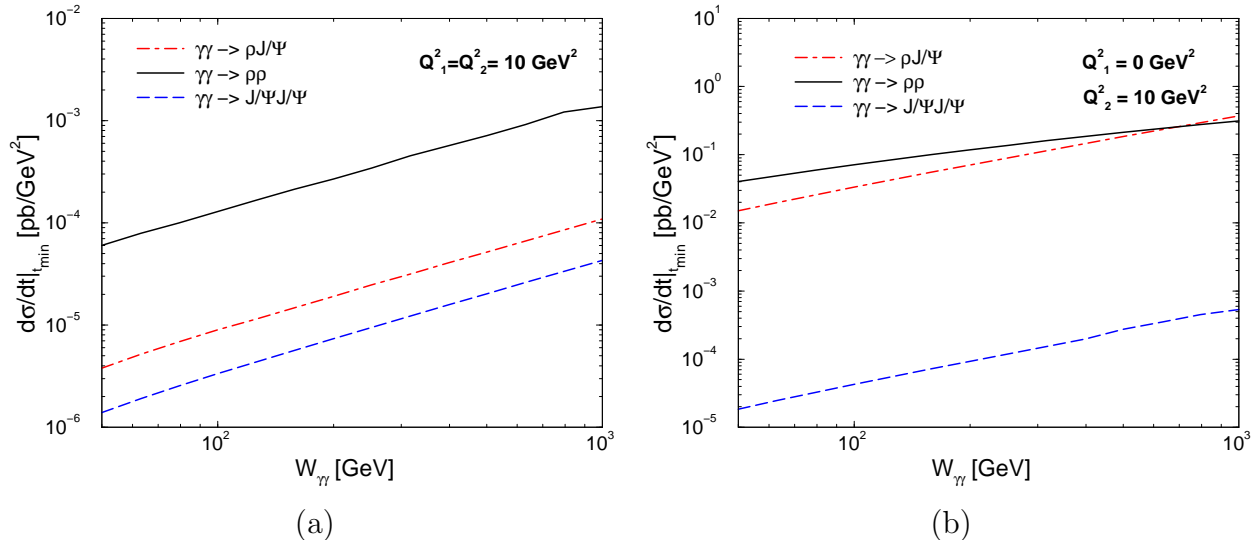


Figure 4: Energy dependence for double vector meson production considering virtual photons considering: (a) equal virtualities ( $Q_1^2 = Q_2^2 = 10 \text{ GeV}^2$ ) and (b) distinct virtualities ( $Q_1^2 = 0$  and  $Q_2^2 = 10 \text{ GeV}^2$ ).

For the double  $J/\Psi$  production,  $\alpha = 1.06$  (0.9), which means  $\alpha_{\mathbb{P}}^{\text{eff}} \approx 0.27$ . Therefore, one has a hard Pomeron behavior in the case where a sufficiently hard scale, the heavy meson mass ( $\bar{\mu}^2 = 4M_{J/\Psi}^2$ ), is present in the problem. Thus, as expected from the phenomenology of  $ep$  collisions, the saturation model for double vector meson production in  $\gamma\gamma$  interactions is able to consistently match the soft behavior when a non-perturbative scale is involved with the hard Pomeron expectations when a perturbative scale is present.

The results presented above can be compared with previous calculations within the color dipole picture. In Ref. [12] there are estimations of the total cross section for double meson production. Our predictions underestimate those results by a factor ten for double  $\rho$  and a factor one hundred for the other mesons. In this comparison we have used the following values for the slope parameters:  $B_{\rho\rho} = 10 \text{ GeV}^{-2}$ ,  $B_{\rho J/\Psi} = 5 \text{ GeV}^{-2}$  and  $B_{J/\Psi J/\Psi} = 0.44 \text{ GeV}^{-2}$ , which are taken from our recent investigations on double meson production in Refs. [15, 16]. The reason for these deviations are probably due to the different dipole-dipole cross section, distinct choices for the quark masses and uncertainties in the determination of the slope parameter. For instance, the dipole-dipole cross section in Ref. [12] behaves as  $\sigma_{dd} \propto r_1^4 r_2^4$  for small dipoles and  $\sigma_{dd} \propto r_1^2 r_2^2$  for large dipoles, which overestimate the integration on dipole sizes in comparison with the dipole-dipole cross sections presented here. Namely, one has  $\sigma_{dd} \propto r_{\text{eff}}^2 Q_{\text{sat}}^2$  for dipoles having transverse size  $r_{\text{eff}} < 1/Q_{\text{sat}}$  and  $\sigma_{dd} \propto \hat{\sigma}_0$  for dipoles of size  $r_{\text{eff}} > 1/Q_{\text{sat}}$ .

### 3.2 Double meson production on virtual photons interactions

Lets now consider the double vector meson production when we have the interaction of two virtual photons. In Fig. 4 (a) we present the predictions of the GBW parameterization for the

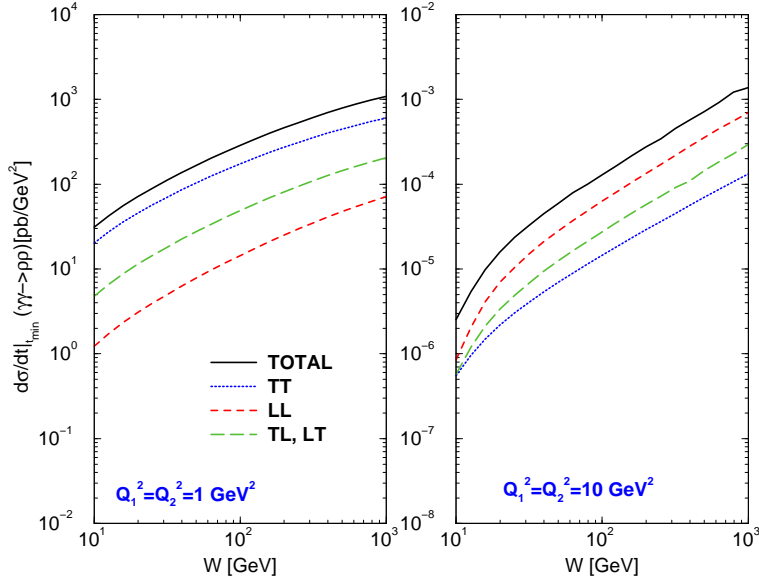


Figure 5: Energy dependence for double  $\rho$  production at equal photon virtualities,  $Q^2 = 1$  and  $Q^2 = 10$  GeV<sup>2</sup>. The contributions of the different polarizations (TT, LL, TL/LT) are explicitly presented. See discussion in text.

energy dependence of the forward differential cross section for double vector meson production considering that the incident photons have equal virtualities ( $Q^2 = 10$  GeV<sup>2</sup>). We have that the forward differential cross section decreases when the virtuality and/or the total mass of the final state are increased. The differential cross sections present a behavior similar on energy, independently of the meson mass. This is due the sufficiently hard scale for these processes given by  $\mu^2 = 2Q^2 + M_{V_1}^2 + M_{V_2}^2$ , which is basically determined by the high photon virtuality, since  $2Q^2 \geq M_V^2$ . This also explains the proximity between the  $\rho J/\Psi$  and double  $J/\Psi$  predictions, in contrast with obtained for the real photon interactions. A power-like fit to the differential cross section in the form  $\left. \frac{d\sigma_{V_1 V_2}}{dt} \right|_{t_{min}=0} \propto W_{\gamma\gamma}^\alpha$  gives  $\alpha = 1.01, 1.08, 1.1$  for double  $\rho$ ,  $\rho J/\Psi$  and double  $J/\Psi$ , respectively. Our result for double  $\rho$  is consistent with the NLA BFKL calculation using BLM scale fixing presented in Ref. [19].

In Fig. 4 (b) we present our predictions for double meson production considering unequal photon virtualities. We consider the limit case of real photon scattering on a deeply virtual partner, namely  $Q_1^2 = 0$  and  $Q_2^2 = 10$  GeV<sup>2</sup>. Now, the typical scale is given by  $\mu^2 = Q^2 + M_{V_1}^2 + M_{V_2}^2$ . We have that the behavior of the different predictions are similar those obtained in Fig. 4 (a), with the energy dependence for  $\rho J/\Psi$  and double  $J/\Psi$  production being almost identical those obtained in the symmetric case. The main difference occurs for double  $\rho$  production, which has its energy dependence strongly modified by saturation effects due to the small value of  $\mu^2$  present in the problem. A power-like fit to the differential cross section in the form  $\left. \frac{d\sigma_{V_1 V_2}}{dt} \right|_{t_{min}=0} \propto W_{\gamma\gamma}^\alpha$  gives  $\alpha = 0.65, 1.03, 1.08$  for double  $\rho$ ,  $\rho J/\Psi$  and double  $J/\Psi$ , respectively.

Using the dipole approach the contribution of the different polarizations for the forward differential cross section can be directly estimated. Lets start considering the double  $\rho$  production

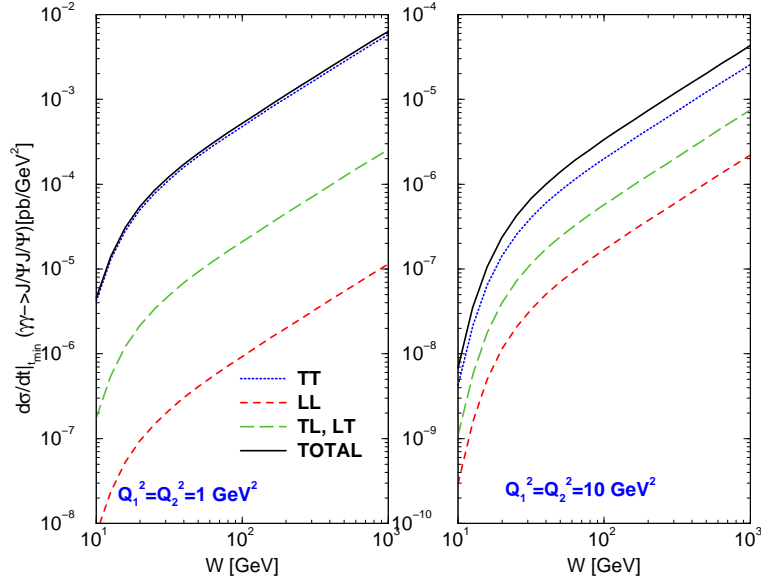


Figure 6: Energy dependence for double  $J/\Psi$  production at equal photon virtualities,  $Q^2 = 1$  and  $Q^2 = 10 \text{ GeV}^2$ . The contributions of the different polarizations (TT, LL, TL/LT) are explicitly presented. See discussion in text.

at equal virtualities of photons. We take the following illustrative cases,  $Q_1^2 = Q_2^2 = 1 \text{ GeV}^2$  and  $Q_1^2 = Q_2^2 = 10 \text{ GeV}^2$ . These choices allow to observe the dependence of each contribution on virtuality. The results are shown in Fig. 5. The transverse piece (TT) is labeled by dotted curves, longitudinal piece by dashed curves, mixed transverse-longitudinal (TL or LT) by long dashed curves and the total cross section (summation over polarizations) by the solid curves. In case of production of a same vector meson, the TL and LT pieces contribute equally,  $TL = LT$ . For virtualities  $Q^2 = 1 \text{ GeV}^2$ , the transverse content dominates, followed by the LT/LT and LL pieces. Longitudinal content is a quite small contribution, which is consistent with the longitudinal wavefunction to be proportional to photon virtuality, which vanishes when  $Q^2 \rightarrow 0$ . A completely different situation occurs when the virtualities increase to  $Q^2 = 10 \text{ GeV}^2$ . In this case the longitudinal piece is dominant, followed by the LT/LT and transverse parts. This is consistent with the ratio  $\sigma_L/\sigma_T \geq 0$  being  $Q^2$ -dependent in the light meson photoproduction (See e.g. Ref. [25]).

A similar analysis can be made for the double  $J/\Psi$  production (see Fig. 6). We take the same virtualities for the virtual photons and equal notation as in the previous analysis. For virtualities  $Q_1^2 = Q_2^2 = 1 \text{ GeV}^2$ , the transverse content dominates, followed by the LT/LT and LL pieces. As in the double  $\rho$  case, the longitudinal contribution is quite small. The total contribution is determined completely by the transverse contribution, with other pieces being negligible. A completely different situation occurs when virtualities increase to  $10 \text{ GeV}^2$  in contrast with the  $\rho$  case. The pattern remains the same as for  $Q^2 = 1 \text{ GeV}^2$ , with transverse piece still dominant, followed by LT/TL and LL pieces. The total contribution is slightly larger than the transverse one.

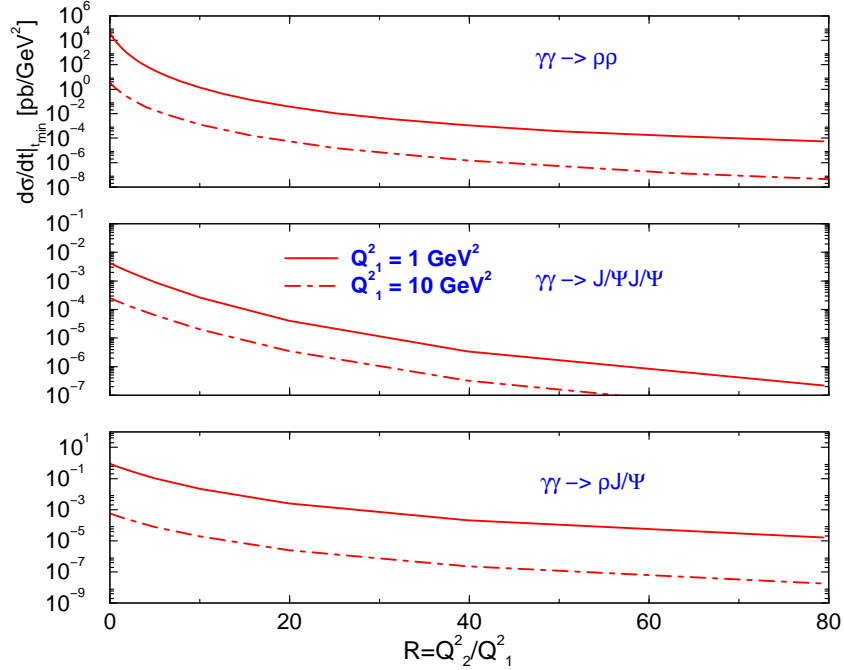


Figure 7: Dependence of the forward differential cross section on the ratio  $R = Q_2^2/Q_1^2$  of photon virtualities at  $Q_1^2$  fixed.

Finally, let's investigate the dependence on virtuality at fixed energy of the forward differential cross section. We take the representative energy of  $W_{\gamma\gamma} = 500$  GeV. In Fig. 7 we present the dependence of the forward differential cross section in the ratio  $R = Q_2^2/Q_1^2$  at fixed  $Q_1^2$  for each vector meson. We take the typical values  $Q_1^2 = 1$  and  $Q_1^2 = 10$  GeV<sup>2</sup>. In all cases, the cross section decreases as  $Q_2^2$  rises, presenting finite values towards  $R = 0$ . It should be mentioned that this interpolation can not be obtained in the BFKL approach in view of the lack of a scale in the process. In our case, the saturation scale provides the needed semihard scale. In order to investigate the quantitative behavior on  $R$  at intermediate virtualities, we adjust the curves with the simple exponential parameterization for  $R \geq 1$  in the form  $\left. \frac{d\sigma_{V_1 V_2}}{dt} \right|_{t_{min}=0} \propto e^{-\beta R}$ . This procedure gives  $\beta = 4.4, 2.6, 2.9$  for double  $\rho$ , double  $J/\Psi$  and  $\rho J/\Psi$ , respectively. The results follow a typical saddle-point BFKL solution in the region of  $R \geq 5$  GeV<sup>2</sup>, namely the cross sections behave as  $\left. \frac{d\sigma_{V_1 V_2}}{dt} \right|_{t_{min}=0} \propto \frac{1}{Q_1^2 Q_2^2} \exp(-\beta \ln^2 R)$  as computed in Ref. [19]. It should be noticed that our definition for  $R$  is slightly different as in that reference.

### 3.3 Investigating saturation effects

Let's now investigate the magnitude of saturation effects in the differential cross section comparing the results using the small  $r_{\text{eff}}$  approximation for the dipole-dipole cross section in contrast with the complete expression including transition to the saturation regime (See discussion in Sect. 2.2). We restrict our analysis to a comparison between the linear and saturation model

predictions for double  $\rho$  and  $J/\Psi$  production. The results are shown in Fig. 8, where solid lines stand for the resummed calculations and dot-dashed one for the linear approximation. It should be noticed that the saturation scale is different for each meson because  $Q_{\text{sat}}^2 \approx (x_0/x_{12})^{0.3}$  and  $x_{12}$  depends on the meson mass as defined in Eq. (1). For the most striking case, in the production by two real photons, the saturation scale for  $\rho$  reaches  $Q_{\text{sat}}^2 \approx 2.5 \text{ GeV}^2$  whereas stays as  $Q_{\text{sat}}^2 \approx 1 \text{ GeV}^2$  for  $J/\Psi$ . Therefore, the saturation scale is higher for  $\rho$  than for  $J/\Psi$  up to intermediate virtualities. Lets start discussing double  $J/\Psi$  production [see Fig 8 (b)], which is one typical hard process characterized by a hard scale given by  $\mu^2(Q, M_V) = 2(Q^2 + M_{J/\Psi}^2)$ . Consequently, we may expect that a perturbative description to be valid even in the real photon limit,  $Q^2 \rightarrow 0$ , and that the contribution from the saturation effects to be small while  $\mu^2 \gg Q_{\text{sat}}^2$ . However, as the saturation scale grows with the energy, the saturation effects become important at large energies. This is the reason we start to see deviations between linear and resummed predictions at  $W \approx 1 \text{ TeV}$  in the real photon case. The results thus indicate that double  $J/\Psi$  production is not to much affected by saturation corrections for energies smaller than 1 TeV. On the other hand, in the double  $\rho$  production the situation changes drastically. For real photons, it is a typical soft process and, therefore, in this case the linear and saturation predictions are very distinct. Now, the scale is given by  $\mu^2(Q, M_V) = 2(Q^2 + M_\rho^2)$ , which should be treated carefully due to the small meson mass. The results are presented in Fig. 8 (a). In the real photon scattering, one has  $\mu^2 = 2M_\rho^2 \approx 1 \text{ GeV}^2$  and therefore saturation effects are increasingly important as  $\mu^2 < Q_{\text{sat}}^2(W_{\gamma\gamma})$ , which explain the reason for the cross section to be reduced by two orders of magnitude at  $W_{\gamma\gamma} \simeq 1 \text{ TeV}$ . At  $Q^2 = 10 \text{ GeV}^2$ , the scenario is different since  $\mu^2 = 2Q^2 \geq Q_{\text{sat}}^2$ . Therefore, the resummed prediction is similar to the linear but corrections for large energies are still important. In view of discussions above, double  $\rho$  production becomes an ideal place to probe the saturation physics.

## 4 Summary

In this paper we have extended the dipole picture for the double vector meson production,  $\gamma^*(Q_1)\gamma^*(Q_2) \rightarrow V_1V_2$ , and calculated the forward differential cross section assuming that the dipole-dipole cross section can be modeled by a saturation model. We have analyzed the energy and virtuality dependence and investigated the magnitude of saturation effects. It is found that the effective power on energy is directly dependent on the typical momentum scale for the process,  $\mu^2 = Q_1^2 + Q_2^2 + M_{V_1}^2 + M_{V_2}^2$ , which is different for distinct meson pair and photon virtualities. Saturation effects are important for double  $\rho$  production on real photons, whereas is small for processes containing  $J/\Psi$  and/or large photon virtualities. It is shown the contribution of the distinct polarizations and its regions of dominance for each meson pair. The results are consistent with expectations from electroproduction of vector mesons. The dependence on virtuality has been investigated using the analysis on the ratio  $R = Q_2^2/Q_1^2$ . The results are qualitatively in agreement with previous predictions obtained using dipole or NLO BFKL approaches. Our results demonstrate that double meson production in two photon interactions at high energies offer an ideal opportunity for the study of the transition between the linear and saturation regimes.

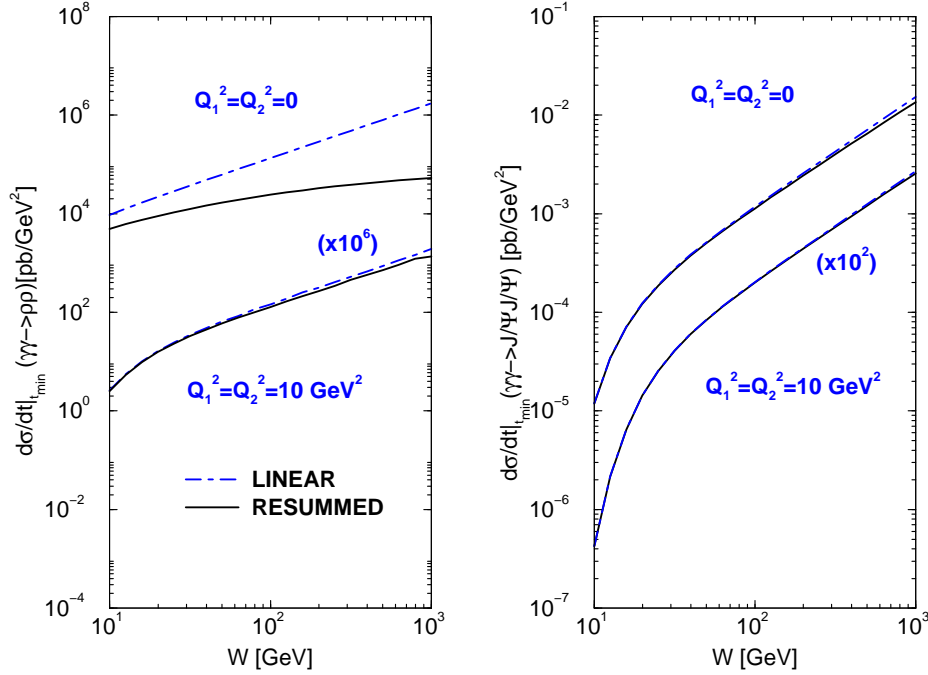


Figure 8: Comparison between the linear and saturation predictions for the energy dependence of the forward differential cross section: (left panel) double  $\rho$  production and (right panel) double  $J/\Psi$  production.

## Acknowledgments

VPG would like to thanks W. K. Sauter for informative and helpful discussions. One of us (M. Machado) thanks the support of the High Energy Physics Phenomenology Group, GFPAE IF-UFRGS, Brazil. This work was partially financed by the Brazilian funding agencies CNPq and FAPERGS.

## References

- [1] L. N. Lipatov, Sov. J. Nucl. Phys. **23**, 338 (1976); E. A. Kuraev, L. N. Lipatov, V. S. Fadin, JETP **45**, 1999 (1977); I. I. Balitskii, L. N. Lipatov, Sov. J. Nucl. Phys. **28**, 822 (1978).
- [2] V.N. Gribov and L.N. Lipatov, Sov. J. Nucl. Phys. **15**, 438 (1972); G. Altarelli and G. Parisi, Nucl. Phys. **B126**, 298 (1977); Yu.L. Dokshitzer, Sov. Phys. JETP **46**, 641 (1977).
- [3] I. Balitsky, Nucl. Phys. B **463**, 99 (1996); Y. V. Kovchegov, Phys. Rev. D **60**, 034008 (1999); Phys. Rev. D **61**, 074018 (2000).



- [4] L. D. McLerran and R. Venugopalan, Phys. Rev. D **49**, 2233 (1994); E. Iancu, A. Leonidov, L. McLerran, Nucl. Phys. A **692**, 583 (2001); E. Ferreiro, E. Iancu, A. Leonidov, L. McLerran, Nucl. Phys. A **703**, 489 (2002); J. Jalilian-Marian, A. Kovner, L. McLerran and H. Weigert, Phys. Rev. D **55**, 5414 (1997); J. Jalilian-Marian, A. Kovner and H. Weigert, Phys. Rev. D **59**, 014014 (1999), *ibid.* **59**, 014015 (1999), *ibid.* **59** 034007 (1999); A. Kovner, J. Guilherme Milhano and H. Weigert, Phys. Rev. D **62**, 114005 (2000); H. Weigert, Nucl. Phys. **A703**, 823 (2002).
- [5] K. Golec-Biernat and M. Wüsthoff, Phys. Rev. D **60**, 114023 (1999); Phys. Rev. D **59**, 014017 (1998).
- [6] J. Bartels, K. Golec-Biernat and H. Kowalski, Phys. Rev. D **66** (2002) 014001.
- [7] H. Kowalski and D. Teaney, Phys. Rev. D **68**, 114005 (2003).
- [8] E. Iancu, K. Itakura and S. Munier, Phys. Lett. B **590**, 199 (2004).
- [9] N. Timneanu, J. Kwiecinski, L. Motyka, Eur. Phys. J. C **23**, 513 (2002).
- [10] N. N. Nikolaev and B. G. Zakharov, Z. Phys. **C49**, 607 (1991); Z. Phys. **C53**, 331 (1992); A. H. Mueller, Nucl. Phys. **B415**, 373 (1994); A. H. Mueller and B. Patel, Nucl. Phys. **B425**, 471 (1994).
- [11] N. N. Nikolaev, J. Speth and V. R. Zoller, Eur. Phys. J. C **22**, 637 (2002); J. Exp. Theor. Phys. **93**, 957 (2001) [Zh. Eksp. Teor. Fiz. **93**, 1104 (2001)].
- [12] A. Donnachie, H. G. Dosch and M. Rueter, Phys. Rev. D **59**, 074011 (1999)
- [13] J. Kwiecinski, L. Motyka, Phys. Lett. B **438**, 203 (1998); Acta Phys. Pol. B **30**, 1817 (1999).
- [14] L. Motyka, B. Ziaja, Eur. Phys. J. C **19**, 709 (2001).
- [15] V. P. Goncalves and M. V. T. Machado, Eur. Phys. J. C **28**, 71 (2003)
- [16] V. P. Goncalves and M. V. T. Machado, Eur. Phys. J. C **29**, 271 (2003).
- [17] V. P. Goncalves and W. K. Sauter, Eur. Phys. J. C **44**, 515 (2005).
- [18] B. Pire, L. Szymanowski and S. Wallon, Eur. Phys. J. C **44**, 545 (2005)
- [19] R. Enberg, B. Pire, L. Szymanowski and S. Wallon, Eur. Phys. J. C **45**, 759 (2006)
- [20] D. Y. Ivanov and A. Papa, Nucl. Phys. B **732**, 183 (2006)
- [21] V. Barone and E. Predazzi, *High-Energy Particle Diffraction*, Springer-Verlag, Berlin Heidelberg, (2002).
- [22] S. Munier, A. M. Stasto and A. H. Mueller, Nucl. Phys. B **603**, 427 (2001).

- [23] J. R. Forshaw, R. Sandapen and G. Shaw, Phys. Rev. D **69**, 094013 (2004).
- [24] H. G. Dosch, T. Gousset, G. Kulzinger and H. J. Pirner, Phys. Rev. **D55**, 2602 (1997).
- [25] N. N. Nikolaev, Comments Nucl. Part. Phys. **21**, 41 (1992); I. P. Ivanov, N. N. Nikolaev and A. A. Savin, arXiv:hep-ph/0501034.
- [26] V. P. Goncalves and M. V. T. Machado, Eur. Phys. J. C **38**, 319 (2004).
- [27] M. Wirbel, B. Stech and M. Bauer, Z. Phys. **C29**, 637 (1985).
- [28] S. J. Brodsky and G. P. Lepage, Phys. Rev. **D22**, 2157 (1980).
- [29] E. Levin and K. Tuchin, Nucl. Phys. B **573**, 833 (2000).